Structural Evolution of Silver Nanoparticles during Wet-Chemical Synthesis

ARTICLE *in* CHEMISTRY OF MATERIALS · JANUARY 2014

Impact Factor: 8.35 · DOI: 10.1021/cm4025342

CHEMISTRY OF MATERIALS

Article

pubs.acs.org/cm

Structural Evolution of Silver Nanoparticles during Wet-Chemical Synthesis

S. Banerjee, K. Loza, W. Meyer-Zaika, O. Prymak, and M. Epple*

Inorganic Chemistry, Center for Nanointegration Duisburg-Essen (CeNIDE), University of Duisburg-Essen, Universitaetsstr. 5-7, 45117 Essen, Germany

ABSTRACT: The formation of silver nanoparticles during the reduction with glucose in the presence of poly(N-vinyl pyrrolidone) as capping agent was followed for more than 3000 min. First, spherical silver nanoparticles are formed, but in later stages, an increasing fraction of nanotriangles and also a few nanorods develop. Both spherical and trigonal nanoparticles grow with time, indicating separate nucleation pathways. The domain size in the spherical nanoparticles increases proportionally to the particle diameter and is always about $^1/_4$ of the diameter, indicating that twinned seeds are formed very early in the process and then simply grow by extending their domains. The lattice constant of the nanoparticles is systematically increased in comparison to microcrystalline silver (4.0877 vs 4.08635 Å) but did not change as a function of particle diameter. A thorough analysis of the texture coefficient, supported by transmission electron microscopy data, showed that the apparently spherical particles are in fact flattened pentagonal prisms, which typically lie on their flat pentagonal face. Neither the presence of oxygen nor the presence of ambient light had any influence on the particle properties.

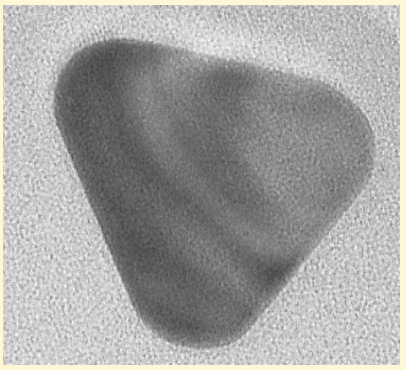

1. INTRODUCTION

The morphological and colloidal characterization of silver nanoparticles has evidenced strong connections between properties such as average particle size, shape, and dispersity with their observed, and inherently tunable physiochemical behavior.[1,2] Nanoparticles constitute a state of matter at the boundary between molecule and bulk material. Accordingly, silver nanoparticles are often engineered in a hierarchy where constituent molecules in a synthesis route serve as the basis for determining the atomic arrangement of silver ions, repeated in an ordered crystal lattice, progressively defining the crystalline ultrastructure of the nanoparticle.[3]

Particle morphology and size distribution can be accurately measured with a variety of techniques, for example, dynamic light scattering (DLS), analytical disk centrifugation, and electron microscopy (scanning and transmission).[4] For most wet-chemical synthesis techniques, such metrics provide the information needed to tailor synthesis conditions by manipulating the reagents that influence the chemical environment during synthesis.[5−8] Other synthesis routes utilize external mediators, ranging from plasmonic excitation to laser ablation.[2,7,9,10] However, regardless of the specific synthesis regime, there is a prevalent emphasis on relating the final morphology of nanoparticles to the chosen experimental parameters in place by analyzing their ultrastructural and crystallographic growth. Given the present hierarchy in nanoparticle structural organization, a more complete understanding of which factors influence the final morphology could be improved by tracking synthesis-specific ultrastructural properties such as domain size and crystallite size, together with measurements of particle size and shape uniformity.[11,12] Additionally for silver nanoparticles, ultrastructural characterization may provide another screening method for controlling the antibacterial and cytotoxic properties of colloids, produced from high yield synthesis routes and geared toward biological applications.[3,13,14]

Although the anisotropic crystal growth of Ag and Au nanoparticles is widely reported, and experimentally controlled, there is a considerable debate regarding which physical and chemical factors influence their often unpredictable and preferential shape development.[7,8,15,16] The two dominant theories that dictate the evolution of particle morphology involve an emphasis on either the crystal structure of the initial "twinned seeds" or the preferential adsorption of capping ligands/surfactants on specific crystallographic facets.[5,6,10,17−23] Additionally, light has been discussed as a parameter that influences the shape of silver nanoparticles.[24]

Here, we report on a comprehensive study on the structure of silver nanoparticles during the reduction of silver ions with glucose. Glucose is a well-known reducing agent for silver. Poly(N-vinylpyrrolidone) (PVP) was used as capping agent. The structural and morphological properties of silver nanoparticles were studied by different methods, especially by electron microscopy and X-ray powder diffraction, during the synthesis.

2. EXPERIMENTAL SECTION

Synthesis of Silver Nanoparticles. PVP-coated silver nanoparticles were synthesized by reduction with glucose in

Received: July 26, 2013
Revised: November 6, 2013
Published: January 7, 2014

the presence of PVP according to Wang et al.[25] Briefly, 16 g glucose and 8 g PVP were dissolved in 320 mL water and heated to 90 °C. Then, 4 g $AgNO_3$ dissolved in 8 mL water were quickly added. The dispersion was kept at 90 °C for different times (up to 7000 min) and then let to cool to room temperature. For partial air exposure, a synthesis in an Erlenmeyer flask covered with a concave hourglass was performed. The system was heated to 90 °C in a silicon oil bath under ambient light exposure. A synthesis without air exposure was carried out in a round-bottom flask with reflux condenser (water cooling) but under exposure to ambient light. To elucidate the role of light exposure, the synthesis under reflux was also carried out under completely dark conditions, that is, protected from irradiation during the whole reaction process. All syntheses were carried out under continuous vigorous stirring. Aliquots of the reaction mixtures were taken after selected time periods. At each point, a 10 mL aliquot of the solution was taken with a syringe. The particles were collected and separated from synthesis byproducts by ultracentrifugation (29 400 g; 30 min), redispersed in pure water, and collected again by ultracentrifugation. This procedure was repeated three times. Thereby, nitrate, excess glucose and its oxidation products, excess PVP, and excess silver ions were removed. After the third cycle, the sample was redispersed in 10 mL of distilled water and analyzed by dynamic light scattering to confirm the absence of agglomerates. All samples were stored at 4 °C in the dark until further analysis. Poly(N-vinylpyrrolidone) (PVP; Sigma-Aldrich, molecular weight 40 000 g mol^{-1}), silver nitrate (Roth, p.a.), and D-(+)-glucose (Fluka, p.a.) were used. Ultrapure water was prepared with an ELGA Purelab ultra instrument.

Analytical Methods. Scanning electron microscopy (SEM) was performed with a FEI Quanta 400 ESEM instrument in high vacuum without sputtering. Ten microliters of a dispersion was dripped on a silicon wafer and dried at room temperature in air. Transmission electron microscopy (TEM) was carried out with a CM200 FEG-Instrument (Philips) with a Supertwin-Lens, operated at an accelerating voltage of 200 keV. The samples were ultrasonically dispersed in ethanol and then transferred to holey carbon-coated copper grids. The hydrodynamic diameter and the zeta potential of the nanoparticles were measured by dynamic light scattering (DLS) using a Malvern Zetasizer Nano ZS. The polydispersity index (PDI) was below 0.3 in all cases. X-ray powder diffraction was carried out on a Bruker D8 Advance instrument in Bragg−Brentano mode with Cu Kα radiation (1.54 Å; 40 kV and 40 mA) using a silicon single crystal with a crystallographic (911)-plane as sample holder to minimize scattering. For better homogenization, the dried powder samples were redispersed with ethanol on the silicon surface and then investigated in the range from 5 to 90° 2θ with a step size of 0.01° 2θ with a counting time of 0.6 s. Rietveld refinement (Le Bail method) with the program package TOPAS 4.2 from Bruker was performed to determine the average crystallite size and the lattice parameters. For each Rietveld refinement, the instrumental correction as determined with a standard powder sample LaB_6 from NIST (National Institute of Standards and Technology) as standard reference material (SRM 660b; $a(LaB_6)$ = 4.15689 Å) was taken into account. The pattern of elemental silver from the ICDD database (#4-0783) was used as reference. The texture coefficient (TC) was calculated using the relationship defined by Barret and Massalski:[26]

$$TC_{(hkl)} = I_{(hkl)}/I_{0(hkl)}/[n^{-1}\sum (I_{(hkl)}/I_{0(hkl)})] \quad (1)$$

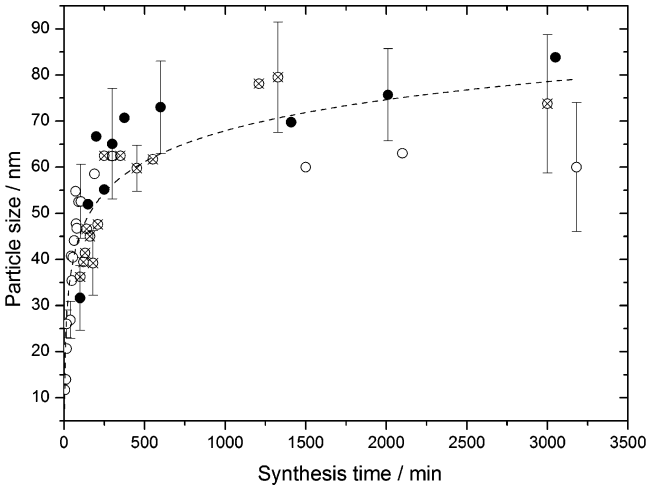

Figure 1. Evolution of the diameter of spherical silver nanoparticles with time as determined by scanning electron microscopy. Open circles: synthesis in air. Crossed circles: synthesis under reflux and ambient light exposure. Closed circles: synthesis under reflux in the dark. Typical standard deviations for the particle diameter are indicated by error bars. For particles with a diameter below 40 nm, the standard deviation is about 7 nm; for larger particles, it is about 16 nm.

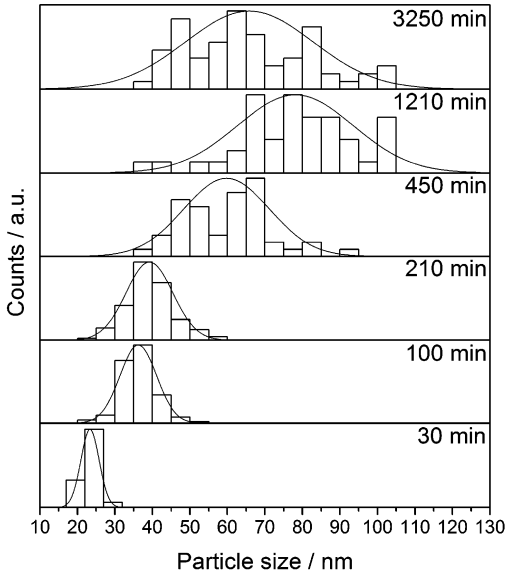

Figure 2. Particle size distribution of the spherical nanoparticles (as diameter) as a function of reaction time. At least 200 individual particles were examined for each time point.

where I is the intensity of the diffraction peaks, $I_{(hkl)}$ and $I_{0(hkl)}$ are the intensities of the (hkl) plane in the diffractograms, measured for the samples and the microcrystalline silver standard (without texture), respectively; n is the number of selected diffraction peaks, and h, k, and l are the Miller indices of the individual crystallographic planes. The summation in the denominator was taken for the first four hkl-planes, that is, (111), (200), (220), and (311). The background was subtracted. As reference, we also studied a microcrystalline silver powder (Fluka, sintered for 3 h at 700 °C to ensure microcrystallinity and absence of microstrain), mixed with LaB_6. All powder diffraction data were obtained at ambient temperature, that is, at 25 ± 2 °C.

dx.doi.org/10.1021/cm4025342 | Chem. Mater. 2014, 26, 951−957

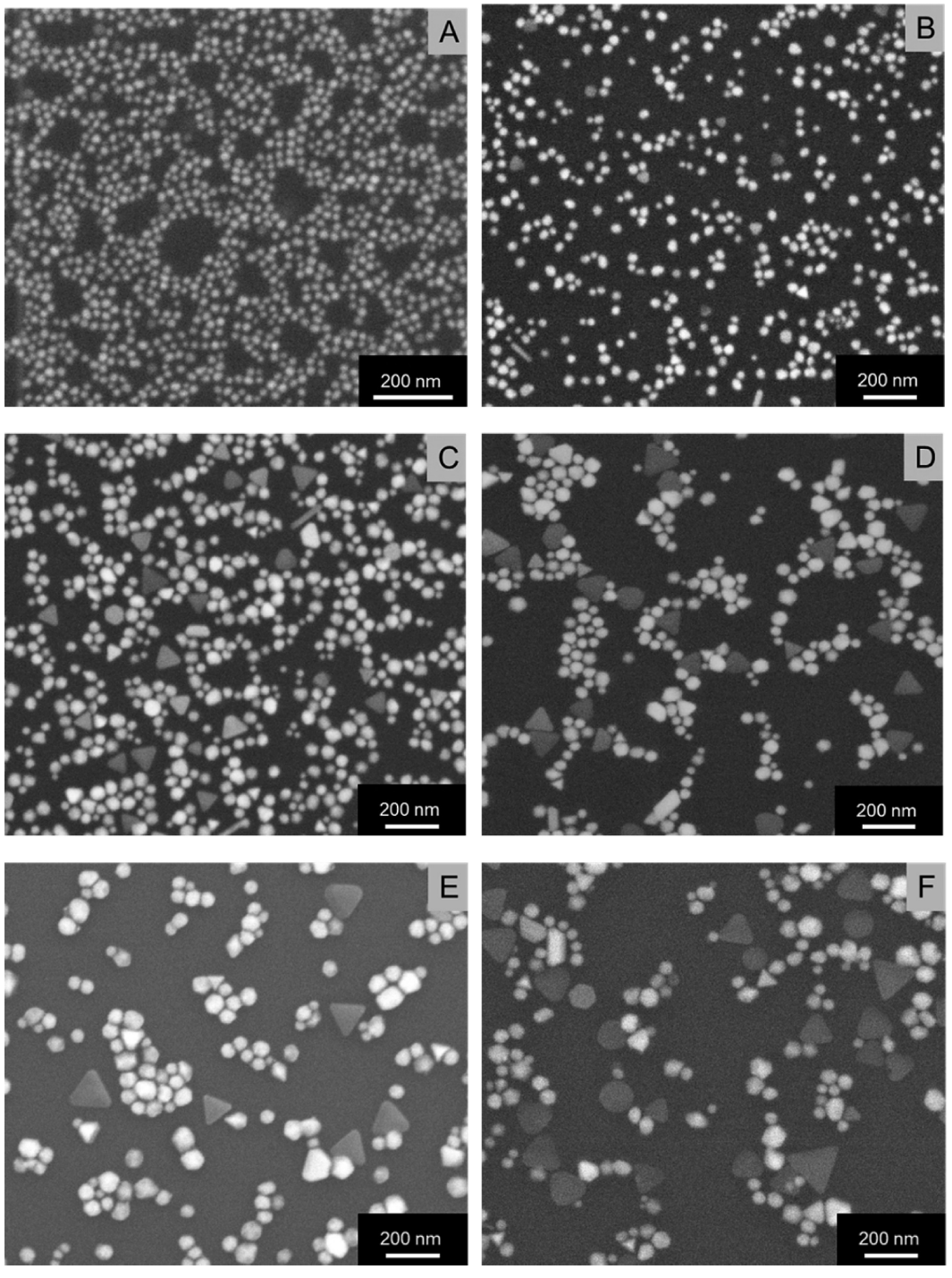

Figure 3. Representative SEM images of silver nanoparticles synthesized under reflux and ambient light exposure after 30 min (A), 100 min (B), 210 min (C), 450 min (D), 1210 min (E), and 3250 min (F).

3. RESULTS AND DISCUSSION

During the synthesis, the diameter of the nanoparticles increases monotonically as shown by dynamic light scattering (DLS) and scanning electron microscopy (SEM). However, to avoid artifacts due to possible agglomeration in DLS and to distinguish between particles of different shape, we derived the particle size from analysis of SEM images. Figure 1 shows the growth of the spherical silver nanoparticles during the synthesis. The particle size was estimated by measuring at least 200 individual spherical particles. We note that the particles grow rapidly in diameter during the first 500 min and then remain practically constant in size. There is no significant difference between the syntheses at different light or air exposure conditions, although the divergence in particle diameters increases for long reaction time.

The particle size distribution of the spherical nanoparticles is shown in Figure 2 for different reaction times. The results indicate that the nucleation occurs mainly at the beginning of the experiment and not continuously, although the particle size distribution becomes broader at longer reaction time.

Figure 3 shows representative scanning electron micrographs of silver nanoparticle samples, taken after different time periods. The diameter of the spherical particles increases with time.

dx.doi.org/10.1021/cm4025342 | *Chem. Mater.* 2014, 26, 951−957

Triangular particles occur first as a small fraction of the particle population but then strongly increase in number and also in size.

The fraction of triangles was quantified by analyzing a large number of particles (>2000). Figure 4 shows that the fraction of

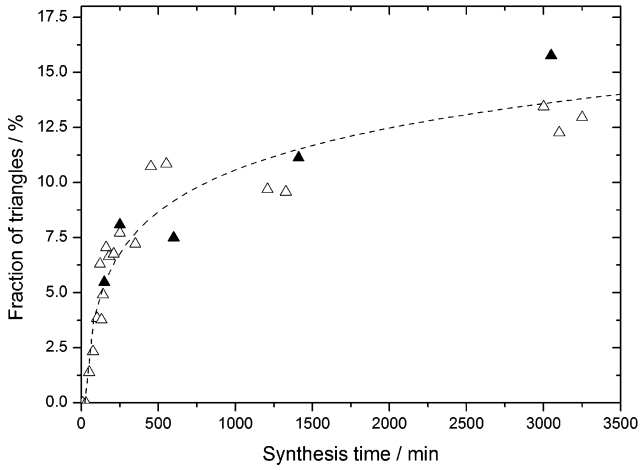

Figure 4. Fraction of triangles on all silver nanoparticles. Open triangles: synthesis under reflux and ambient light exposure. Closed triangles: synthesis under reflux in the dark.

triangles increases with the time. Furthermore, we note that silver triangles can be observed already in the early stages of synthesis, although only as a very small fraction of the particle population. The fraction of triangles is rapidly increasing during the first 500 min. After 3500 min around 13% of particles are triangles. The presence or absence of light has no significant effect on the particle shape.

Scanning electron images show geometrically well-defined flat silver triangles. The triangle edge length also increases

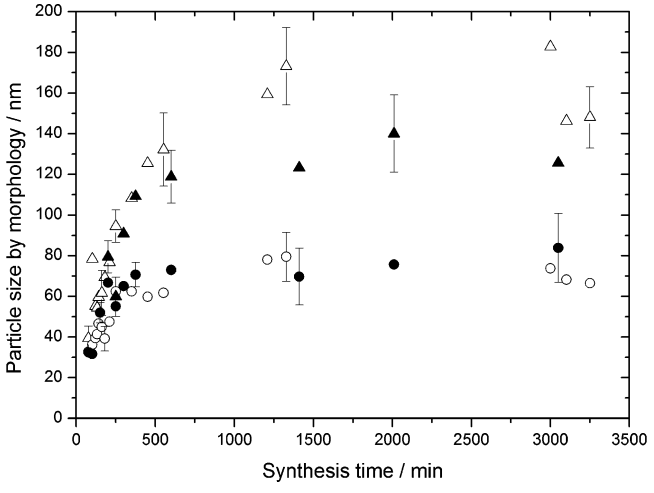

Figure 5. Particle size for different morphologies vs time: spheres (maximum diameter) and triangles (edge length of a perfect triangle). Open circles: spherical particles from the synthesis under reflux and ambient light exposure. Open triangles: triangular particles from the synthesis under reflux and ambient light exposure. Closed circles: spherical particles from the synthesis under reflux in the dark. Closed triangles: triangular particles from the synthesis under reflux in the dark. Typical standard deviations for the particle diameter (spheres) or edge length (triangles) are given as error bars. For particles with a diameter below 40 nm, the standard deviation is about 7 nm; for larger particles, it is about 16 nm.

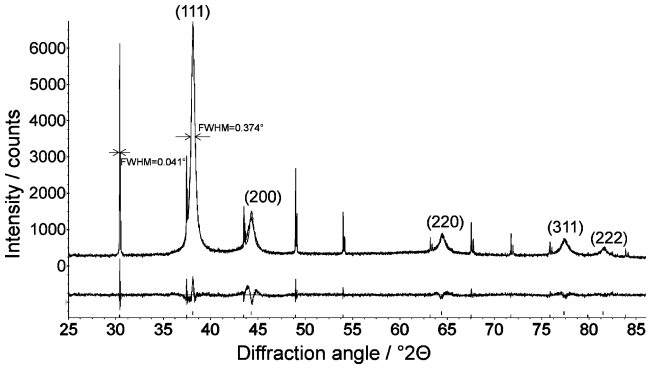

Figure 6. Representative X-ray powder diffractogram (with Rietveld refinement, R_{wp} = 6.6) of a mixture of silver nanoparticles with the microcrystalline standard LaB_6. Note the considerably increased peak width for the silver nanoparticles in comparison with the narrow peaks of the LaB_6 standard. The silver peaks are denoted by their lattice plane indices.

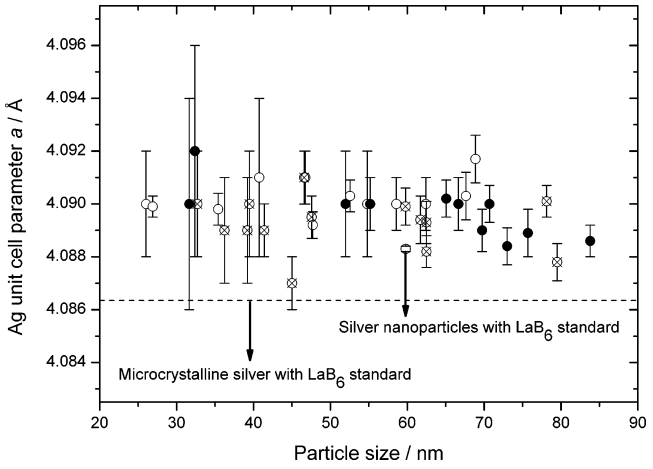

Figure 7. Unit cell parameter *a* vs particle size as determined by dynamic light scattering including error bars. Open circles: synthesis in air under ambient light exposure. Crossed circles: synthesis under reflux and ambient light exposure. Closed circles: synthesis under reflux in the dark. The circled value at 60 nm corresponds to a sample measured with the internal standard LaB_6. The dashed line corresponds to microcrystalline silver, measured with the internal standard LaB_6.

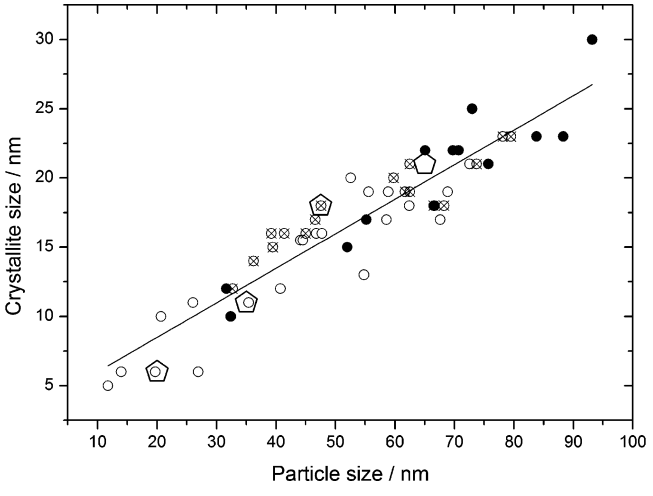

Figure 8. Crystallite size from X-ray powder diffraction vs particle size from dynamic light scattering. Open circles: synthesis in air under ambient light exposure. Crossed circles: synthesis under reflux and ambient light exposure. Closed circles: synthesis under reflux in the dark. The four open pentagons denote domain sizes as derived from TEM data (see Figure 9A–D).

dx.doi.org/10.1021/cm4025342 | *Chem. Mater.* 2014, 26, 951–957

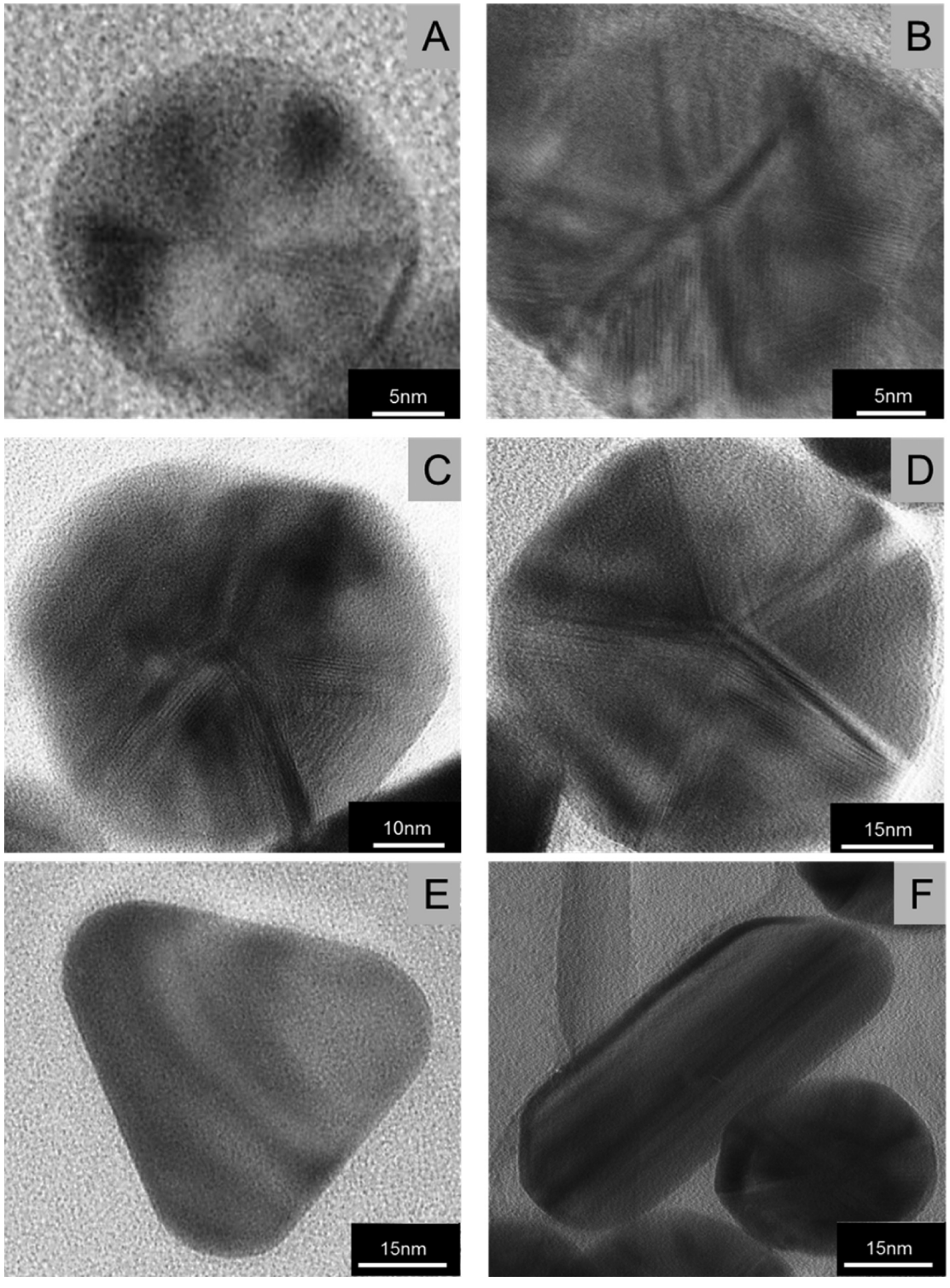

Figure 9. Representative TEM images of silver nanoparticles synthesized under reflux and ambient light exposure after 15 min (A; diameter 20 nm/domain size 6 nm), 42 min (B; 35 nm/11 nm); 65 min (C; 48 nm/18 nm); 350 min (D; 65 nm/21 nm). (E) Representative image of a triangular particle. (F) Representative image of a rod-like particle.

continuously during the synthesis (Figure 5) to about 140 nm after 1000 min. At the same time, the spherical particles reach diameter of only 65 nm. Again, light exposure does not have a significant effect. It is clear, however, that spheres and triangles originate from separate nucleation steps with different nucleation and growth kinetics. The thickness of the particles could neither be determined by SEM (because it was too small) nor by TEM (because it was impossible to orient the flat triangles perpendicular to the electron beam). In a similar study, Zhang et al. have determined the thickness of silver nanoplates by AFM to be below 10 nm, which appears to be realistic in our case as well.[16]

The crystallographic properties of the nanoparticles were analyzed by X-ray powder diffraction. For an accurate

dx.doi.org/10.1021/cm4025342 | *Chem. Mater.* 2014, 26, 951−957

determination of the unit cell parameter a of silver, we mixed a nanoparticle sample with the LaB_6 standard before the diffraction experiment Figure 6 shows a representative X-ray powder diffractogram with narrow peaks from LaB_6 and broad peaks from nanocrystalline silver. By this method, we were able to determine the silver crystallite size to 24 nm and the silver unit cell parameter a with 4.0877(2) Å.

Figure 7 shows the unit cell parameter a of silver nanoparticles as a function of diameter. This was determined without LaB6-standard, therefore the standard deviations are higher for the individual data points due to uncertainties of the measurement, for example, the sample displacement error.[27] For microcrystalline silver mixed with LaB_6, we found a = 4.08635 Å, in good agreement with literature data (4.0862 Å[28] and 4.086 Å[29]). The lattice of the nanoparticles is significantly expanded in comparison to microcrystalline silver, but there is no significant variation in the unit cell parameter of nanoparticles as a function of their size and also no influence of air or light exposure.

Rietveld analysis gave the crystallite size of the nanoparticles from X-ray diffraction peak broadening (Figure 8). The nanoparticle crystallite size displays a linear correlation ($y = 0.25x + 3.5$; $R^2 = 0.86$) between particle size and crystallite size. The Rietveld data are in excellent agreement with TEM data on the domain size (see below). This indicates that under these reducing conditions, the nucleation leads to multiply twinned nanoparticles with domains that are of course smaller than the particle diameter. During the silver nanoparticle growth, the domains grow as well, but the domain structure of the nanoparticles remains unchanged. Otherwise, we would not observe a linear correlation between domain size and particle diameter. If secondary nucleation would occur, the domain size would increase slower than the particle diameter. Notably, there is again no effect of air or light exposure.

The Rietveld analysis averages over many particles without being able to discriminate between individual particles of different size and shape. However, as the spheres constitute the majority of the particle population and as they are rather uniform in size, we can safely assume that X-ray diffraction gives a reasonable estimate of the domain size of the spherical particles.

Further evidence comes from transmission electron microscopy (TEM) of individual nanoparticles (Figure 9). This provides a direct measure of the domain size, as discernible from grain-boundaries between tetrahedra within the particle ultrastructure.[7] Measures of the average domain size from TEM agree well with the crystallite size calculated with the Rietveld method. In TEM, we observed a 5-fold symmetry of the domains, indicating that the particles actually consist of pentagonal bipyramids. For extended reaction time, triangular platelets and also few rod-like particle evolve. Both appear to consist of only one crystallographic domain. This is in sharp contrast to the spherical particles which are always twinned. We never observed nontwinned spherical particles, which indicates that twinning occurs very early during the nucleation.

The texturing of the nanoparticle samples can also be assessed by Rietveld analysis (Figure 10). It is notable that we have a strong preferential orientation from the beginning, which monotonically increases with time, leading to an over-representation of (111) faces in comparison to (200) faces. This can be partly explained by an increasing number of triangular plates, which are most likely oriented with the (111) face parallel to the sample holder, but there must be an additional effect. The fact that the texture coefficient changes consistently with a large number of samples precludes that this is just a statistical effect from

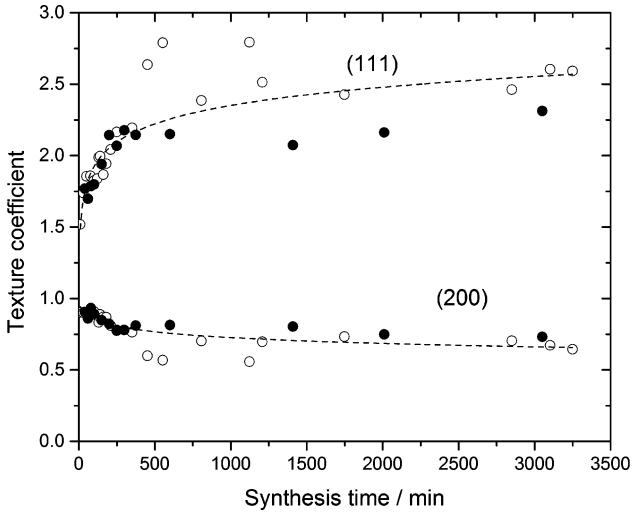

Figure 10. Texture coefficient for syntheses under reflux and ambient air exposure (open circles) and syntheses under reflux in the dark (closed circles) are given for the planes (111) and (200). There is a considerable texture effect which increases rapidly for the (111) plane at early synthesis times and leads to a plateau after about 500 min. At the same time, the diffraction intensity in the (200) direction decreases. This indicates an increasing amount of triangular plates and also underscores the fact the spheres are in fact not spheres but pentagonal bipyramids.

sample drying. We ascribe this effect to the nature of the spherical particles, which are almost always pentagonal twins in the TEM. If a pentagonally twinned crystal would be present in strictly spherical shape, it would orient statistically, and the 5-fold symmetry would not show up in all cases. Of course, in a multilayer of particles, the orientation will not be as perfect as in a monolayer, but this effect is clearly seen in the diffraction data and corroborated by typical results on preferred orientation for nonspherical particles.[27]

Therefore, we propose that these particles are not really spherical but rather flattened pentagonal bipyramids ("UFO-shaped"). This cannot be proven from SEM images due to limited resolution, but we draw such evidence from TEM images where we can see such particles from the side (Figure 10). Such flattened particles will preferably orient on a flat surface with the pentagonal face and lead to a texturing in the (111) direction. Seen from the top, they will appear as spheres (as in the SEM; see Figure 3). From the TEM data shown in Figure 11, we assume that the thickness of the pentagonal twins is about half of their diameter.

The effects of the reducing agent glucose and the capping agent PVP were not investigated in this study. However, these are standard synthetic conditions and reagents which often lead to nanoparticles with different size and shape. Our results show that there are considerable dynamics in the system, up to about 1000 min reaction time. Nucleation appears to occur in early stages, with an imprinting of the final morphology: Sphere (in fact: pentagonal twin) or triangle. These initially formed nuclei (or seeds) grow with time by attracting more silver ions from the solution, but their internal crystallographic structure remains all the same. The different growth rates of spheres and triangles must be related to different kinetics of reduction of silver ions and subsequent attachment onto the silver particle surface.

We wish to note, however, that it is not possible to obtain a fully comprehensive account of all particles with their shapes and

dx.doi.org/10.1021/cm4025342 | Chem. Mater. 2014, 26, 951−957

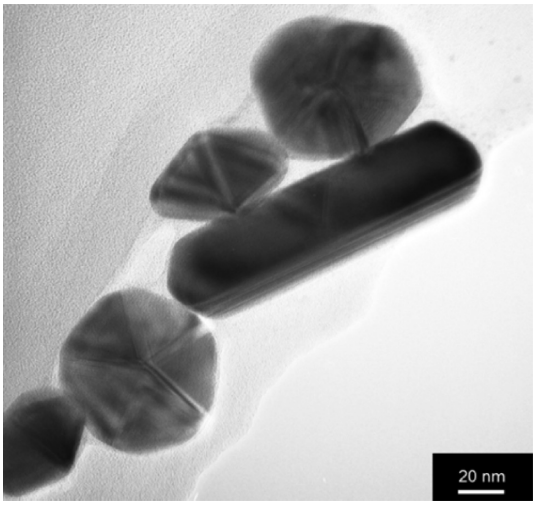

Figure 11. Transmission electron micrograph of a representative sample of silver nanoparticles (350 min under reflux and ambient light exposure), showing one rod-like particle and four pentagonally twinned particles, two from the top and two from the side. The latter are spherical only if seen from the top, but if seen from the side, they are obviously flattened and not of pentagonal symmetry.

sizes during the experiment. Therefore, it cannot be ruled out that some nanoparticles are also nucleated at later stages or that some interconversion or even dissolution (similar to Ostwald ripening) of particles occurs during the course of the reaction.

4. CONCLUSIONS

The reduction of silver with glucose in the presence of PVP leads mostly to spherical nanoparticles, but triangles also occur at a very early stage. Their fraction increases with increasing reaction time. Also, a few rod-like particles are observed at later stages. It is remarkable that both spherical and triangular particles continue to grow during the synthesis and that they seem to originate from different nucleation events. After about 1000 min, the dynamics of the system appear to have ceased. By transmission electron microscopy, the apparently spherical nanoparticles are identified as pentagonally twinned crystals which typically lie on the pentagonal face on a flat surface. The increase of the domain size is proportional to the particle size, indicating that the nanoparticles just grow in size, together with their domains. The silver lattice unit cell parameter a is significantly increased in the nanoparticles by about 0.002 Å. Neither air exposure nor ambient light had a significant effect on the reaction products.

AUTHOR INFORMATION

Corresponding Author

*E-mail: matthias.epple@uni-due.de.

Author Contributions

The manuscript was written through contributions of all authors. All authors have given approval to the final version of the manuscript.

Notes

The authors declare no competing financial interest.

ACKNOWLEDGMENTS

We thank the Deutsche Forschungsgemeinschaft (DFG) for funding this research in the framework of the priority program 1313. S.B. thanks the U.S. Fulbright Foundation for a Student Grant.

REFERENCES

(1) Arumugam, S. K.; Sastry, T. P.; Sreedhar, B.; Mandal, A. B. *J. Biomed. Mater. Res. A* **2007**, *80*, 391−398.
(2) Krutyakov, Y. A.; Kudrinskiy, A. A.; Olenin, A. Y.; Lisichkin, G. V. *Usp. Khimii.* **2008**, *77*, 242−269.
(3) Stark, W. J. *Angew. Chem.* **2011**, *123*, 1276−1293.
(4) Mahl, D.; Diendorf, J.; Meyer-Zaika, W.; Epple, M. *Coll. Surf. A: Physicochem. Eng. Aspects* **2011**, *377*, 386−392.
(5) Wiley, B.; Sun, Y.; Xia, Y. *Acc. Chem. Res.* **2007**, *40*, 1067−1076.
(6) Xia, X.; Zeng, J.; Oetjen, L. K.; Li, W.; Xia, Y. *J. Am. Chem. Soc.* **2012**, *134*, 1793−1801.
(7) Xia, Y.; Xia, X.; Wang, Y.; Xie, S. *MRS Bull.* **2013**, *38*, 335−344.
(8) Xia, Y. N.; Xiong, Y.; Lim, B.; Skrabalak, S. E. *Angew. Chem., Int. Ed.* **2009**, *48*, 60−103.
(9) Sun, Y. G.; Xia, Y. N. *Science* **2002**, *298*, 2176−2179.
(10) Millstone, J. E.; Hurst, S. J.; Metraux, G. S.; Cutler, J. I.; Mirkin, C. A. *Small* **2009**, *5*, 646−664.
(11) Chen, Y.; Zhang, Y.; Chen, J.; Sun, X. *Cryst. Growth Des.* **2011**, *11*, 5457−5460.
(12) Viswanath, B.; Kundu, P.; HaIder, A.; Ravishankar, N. *J. Phys. Chem. C* **2009**, *113*, 16866−16883.
(13) Lee, D. E.; Koo, H.; Sun, I. C.; Ryu, J. H.; Kim, K.; Kwon, I. C. *Chem. Soc. Rev.* **2012**, *41*, 2656−2672.
(14) Chernousova, S.; Epple, M. *Angew. Chem., Int. Ed.* **2013**, *52*, 1636−1653.
(15) Rocha, T. C. R.; Zanchet, D. *J. Phys. Chem. C* **2007**, *111*, 6989−6993.
(16) Zhang, Q.; Hu, Y.; Guo, S.; Goebl, J.; Yin, Y. *Nano Lett.* **2010**, *10*, 5037−5042.
(17) Yu, D. B.; Yam, V. W. W. *J. Phys. Chem. B* **2005**, *109*, 5497−5503.
(18) Marks, L. D. *Rep. Prog. Phys.* **1994**, *57*, 603−649.
(19) Rocha, T. C. R.; Winnischofer, H.; Westphal, E.; Zanchet, D. *J. Phys. Chem. C* **2007**, *111*, 2885−2891.
(20) Zhang, Q.; Li, N.; Goebl, J.; Lu, Z. D.; Yin, Y. D. *J. Am. Chem. Soc.* **2011**, *133*, 18931−18939.
(21) Yin, Y. D.; Li, Z. Y.; Zhong, Z. Y.; Gates, B.; Xia, Y. N.; Venkateswaran, S. *J. Mater. Chem.* **2002**, *12*, 522−527.
(22) Tsuji, M.; Gomi, S.; Maeda, Y.; Matsunaga, M.; Hikino, S.; Uto, K.; Tsuji, T.; Kawazumi, H. *Langmuir* **2012**, *28*, 8845−8861.
(23) Maillard, M.; Huang, P. R.; Brus, L. *Nano Lett.* **2003**, *3*, 1611−1615.
(24) Jin, R.; Cao, Y.; Mirkin, C. A.; Kelly, K. L.; Schatz, G. C.; Zheng, J. G. *Science* **2001**, *294*, 1901−1903.
(25) Wang, H.; Qiao, X.; Chen, J.; Ding, S. *Coll. Surf. A: Physicochem. Eng. Aspects* **2005**, *256*, 111−115.
(26) Barret, C.; Massalski, T. B. *Structure of Metals*; Pergamon Press: Oxford, 1980.
(27) Klug, H. P.; Alexander, L. E. *X-ray Diffraction Procedures for Polycrystalline and Amorphous Materials*. Wiley-Interscience: New York, 1974.
(28) Swanson, H. E. *Nat. Bureau Standards (U.S.), Circular* **1954**, *539*, 3.
(29) Suh, I. K.; Ohta, H.; Waseda, Y. *J. Mater. Sci.* **1988**, *23*, 757−760.